# Tribological properties of cold-sprayed 7075Al coatings reinforced with hybrid nano-TiB2/micro-SiC particles

Shaowu Liu, Hongjian Wu, Xinliang Xie, Gang Ji, Michel Moliere, Hanlin Liao

# Tribological properties of cold-sprayed 7075Al coatings reinforced with hybrid nano-$TiB_2$/micro-SiC particles

Shaowu Liu [a, d, 1], Hongjian Wu [c,*, 1], Xinliang Xie [b,*], Gang Ji [d], Michel Moliere [a], Hanlin Liao [a]

[a] ICB UMR 6303, CNRS, Univ. Bourgogne Franche-Comté, UTBM, F-90010 Belfort, France
[b] Key laboratory for Light-weight Materials, Nanjing Technology University, 211816 Nanjing, China
[c] Institute of Materials Technology, Helmut Schmidt University/University of the Federal Armed Forces Hamburg, 22043 Hamburg, Germany
[d] Unité Matériaux et Transformations (UMET, UMR CNRS 8207), Université de Lille, 59655 Villeneuve d'Ascq, France

ARTICLEINFO

*Keywords:*
Al matrix composites
Cold spray
Tribological
Mechanical properties
Hybrid reinforcements

ABSTRACT

In this study, strategies to strengthen 7075Al matrix by blending involving nano-sized $TiB_2$ and micro-sized SiC particles were investigated in order to prepare advanced, highly wear-resistant Al matrix composites. Cold spray (CS) technology was used to deposit a $TiB_2$/SiC-7075Al composite coating. For comparison purposes, three additional coatings with different powder compositions were produced using the same CS processing parameters. They were pure 7075Al, $TiB_2$/7075Al composite and SiC-7075Al composite coatings, respectively. The mechanical properties, including hardness, modulus, adhesion strength and wear resistance, were examined. The powders and their corresponding coatings, as well as the wear tracks on the coating surfaces, were observed and analyzed by optical microscopy, scanning electron microscopy and energy-dispersive spectroscopy. Results showed that the in-situ formed $TiB_2$ particles were uniformly distributed in the 7075Al matrix, while the ex-situ deposited SiC particles were mainly distributed at inter-particle boundaries. The hybrid reinforced $TiB_2$/SiC-7075Al composite coating exhibited the highest hardness and modulus. The tribological tests showed that both $TiB_2$ and SiC particles greatly influenced the wear behavior of the composite coatings, with the latter having a more significant effect. Dual reinforcement with $TiB_2$ and SiC particles enabled the $TiB_2$/SiC-7075Al composite coating to possess the best tribological properties.

## 1. Introduction

The reinforcement of Al matrix composites (AMCs) with selected ceramics yields high strength, as well as wear and corrosion resistant composites, representing very promising materials for automotive, aircraft, and aerospace applications [1,2]. As a general empirical feedback, the mechanical properties of AMCs are directly related to the processing methods employed. To date, several techniques for preparing AMCs have been successfully practiced, including powder metallurgy [3], melting techniques [4], squeeze casting [5], etc. According to the morphology of the reinforcing materials, AMCs can be classified into three categories: continuous fiber reinforced AMCs, whisker or short fiber reinforced AMCs, and particle-reinforced AMCs (P-AMCs) [2,6,7]. Of these, P-AMCs are of great interest due to their relatively low production cost and isotropic properties.

Cold gas dynamic spray or simply cold spray (CS) is a relatively new solid-state coating technology that allows the deposition of high quality coatings on a variety of substrates [8]. In CS process, powders consisting of particles ranging between 10 and 100 μm are accelerated to very high velocities (500–1200 m/s) by a convergent-divergent de-Laval nozzle under high pressure and low temperature gas [9]. When these particles impact the substrate, they undergo plastic deformations and form a dense coating. The unique low temperature feature of CS makes it possible to prevent or greatly reduce the adverse effects of overheating, such as oxidation, grain growth, residual tensile stress, phase changes and other typical heat-related defects. In other words, CS is able to retain the original properties of the feedstock powder and also avoiding thermal damages to the underlying substrate material [9]. Therefore, CS could be a technique of choice for depositing a wide range of traditional and advanced materials, especially for temperature sensitive materials. Moreover, it is also suitable for non-traditional applications such as the rapid repair of damaged metal parts and the fabrication of free-standing

* Corresponding authors.
*E-mail addresses:* wuh@hsu-hh.de (H. Wu), xinliang.xie@njtech.edu.cn (X. Xie).
[1] These authors have equal contributions to this work.

metal components [10–12].

Over the past few decades, P-AMCs deposited by CS have gained increasing interest owing to their great potential for applications in various fields. This success can be illustrated by three references: (i) CS based ceramic reinforced AMCs were proposed for aircraft component repair [13,14]; (ii) N.H. Tariq et al. [15] fabricated thick $B_4C$/AMCs through CS for neutron shielding applications; (iii) Tao et al. [16] developed Al/α-Al2O3 composite coatings by using CS for corrosion protection of magnesium alloys. To date, various P-AMC coatings have been tentatively deposited by CS in order to improve the mechanical properties of Al (or its alloys) matrices. A wide range of ceramic particles such as SiC, $B_4C$, TiC, $Al_2O_3$, NaCl, $TiO_2$, MgO, $Si_3N_4$, AlN, BN, $TiB_2$, etc. has been widely used as reinforcers for producing AMCs. Among them, SiC is the most commonly used owing to its excellent mechanical properties, such as superior hardness and wear resistance. For instance, Lee et al. [17] investigated the deposition of Al-SiC on Si substrates, using the CS technique. Kunar et al. [18] studied the microstructure and performance of cold-sprayed Al-SiC composite coatings sprayed by CS. He showed that SiC could improve the mechanical properties and wear resistance of these coatings without the risk of thermal decomposition. Meanwhile, the use of CS process allowed hard ceramic particles to act as a blast when impacting on the surface of the coating. Such effect was likely to further increase the hardness and density of the coating. Yu. et al. [19] also produced SiC reinforced 5056Al composite coatings using CS and used feedstock powders containing different volume fractions of SiC particles. Their results showed that the coating deposition efficiency initially increased with the increase of the SiC content in the feedstock, reaching a maximum value when the content of SiC in the feedstock is 45 vol%. In addition, $TiB_2$ is considered to be an excellent candidate to strengthen the matrix of Al or its alloys thanks to its high melting point, hardness, modulus as well as its high tribological performances [20]. In a previous study, a novel in-situ nano-$TiB_2$ reinforced 7075Al powder was developed and used to deposit thick and dense AMCs by CS [21,22]. The structural integrity and dispersion of the nano-$TiB_2$ reinforcing particles was well retained in the coatings. However, the mechanical properties have not been adequately investigated, especially the tribological aspects.

Generally speaking, the mechanical properties of P-AMCs are determined by the type of reinforced particles, their average size and size distribution, the volume fraction of the reinforcing material as well as the nature of the matrix/reinforcement interface [6]. Interestingly, it is possible to use two or more reinforcement materials to enhance and optimize the performance of AMCs. Gurcan and Baker [23] examined the dry sliding and abrasive wear behavior of Al/SiCp, Al/$Al_2O_3$ and Al/($Al_2O_3$ SiCp) hybrid composites. They found better wear resistances with hybrid composites than with composites involving only SiCp or $Al_2O_3$ as reinforcing material. Similarly, Park [24] and H. Ahlatci et al. [25] reported that Al/($Al_2O_3$ + SiC) hybrid composites had better wear resistance than the Al/SiC and Al/$Al_2O_3$ composites. Although, numerous composites with different hybrid materials have been investigated, the preparation via CS and the properties of aluminium-based hybrid composites involving nano-$TiB_2$ and SiC powders as reinforcing components is a subject that has been little explored.

This work builds on previous research [21,22] and continues the development of advanced AMCs using CS technology. By incorporating both $TiB_2$ nanoparticles and micron-sized SiC particles into the 7075Al matrix, AMC coatings were prepared by CS. Comparative coatings were also prepared to reveal the effect of different reinforcement materials on the properties of the final 7075Al hybrid composites. Their microstructures and mechanical properties (mainly their tribological properties) were investigated. This paper also offers a detailed discussion of the wear mechanisms that prevail in the cases of reinforcements by nano-dispersion and micro-particles.

## 2. Experimental details

### 2.1. Cold spray coatings

Mechanical mixing is an easy, efficient and popular method for preparation of composite powders. In this work, SiC powder was mechanically mixed both with 7075Al powders and $TiB_2$/7075Al composite powders. Both 7075 Al powders and $TiB_2$/7075Al composite powders were obtained by atomization under inert gas. The fabrication details of the gas-atomized $TiB_2$/7075Al composite powder can be found in a previous paper [21]. According to another previous study [19], 30 vol% SiC particles were mixed into the feedstock to optimize the deposition efficiency of SiC. The morphologies of the initial matrix powders, i.e., the 7075Al powder and the $TiB_2$/7075Al composite powder, are shown in Fig. 1 a and b, respectively. Both powders exhibit a spherical shape with some local micro-satellite structure. Their cross-sectional images (as shown in Fig. 1 c and d) reveal small grains inside them. The ultra-fine $TiB_2$ particles were uniformly distributed inside the TiB2/7075Al composite particles. Fig. 1 e and f show micrographs of the mechanically mixed powders of 7075Al-SiC and $TiB_2$/7075Al-SiC, respectively. The irregularly shaped SiC powders were well dispersed in the corresponding matrix powders Thus, the matrix powder and the reinforcing powder were uniformly distributed in the feedstock. Furthermore, the mechanical mixing had barely any effect on the morphology of the initial powders. Fig. 2 illustrates the distribution of particle diameters. The 7075Al and $TiB_2$/7075Al composite powders had similar particle size ranges, and their average sizes were 33 and 37 μm, respectively. The average size of SiC powder was 29 μm.

The 7075Al-SiC composite and $TiB_2$/7075Al-SiC hybrid composite coatings, as well as the pure 7075 coating and $TiB_2$/7075Al composite coatings were produced on pre-sand-blasted 7075Al-T6 substrate plates by using a CS system (Kinetics 3000, original CGT GmbH, Germany). The nozzle used has an expansion ratio of 3.8 and a divergent section length of 170 mm. The driving gas is air compressed at 3.0 MPa. The gas temperature is 550 °C. The standoff distance between the substrate and the nozzle exit was set as 30 mm. The nozzle traverse speed during coating deposition was 100 mm/s.

### 2.2. Coating characterization

The microstructures of the powders and coatings were observed using an optical microscope (OM, Nikon, Japan) and scanning electron microscope (SEM, JSM 5800LV, JEOL, Japan) equipped with energy dispersive spectroscopy (EDS). The $TiB_2$ and SiC contents in the composite coatings were estimated using the Scion Image software with at least 10 cross-sectional micrographs.

### 2.3. Microhardness and nanoindentation test

The coating microhardness was measured by a Vickers hardness indenter (Leitz, Germany) with a load of 100 g applied for 10 s. Ten positions were randomly tested on both the cross-section and top surface of the coatings to obtain an average HV0.1 value. The indentation tests on the cross-sections of the coatings were conducted with a G200 nano indenter (Agilent, USA), under a maximum load of 10 mN, a constant indentation loading rate of 0.6 μN/s and a hold time of 10 s. A total of 20 nominally identical indentation tests were carried on each coating to obtain the average nano hardness and the modulus values.

### 2.4. Adhesion test

The adhesion strength on the coating/substrate interface was evaluated according to ASTM-633. A coating with a thickness of 300 μm was deposited on 7075 Al-T6 cylindric substrates with a diameter of 25.4 mm and a thickness of 10 mm. A tensile tester (IC ESCOFFIER, Escotest 50, France) was used to pull-out the adhesion samples at a speed of 1.26

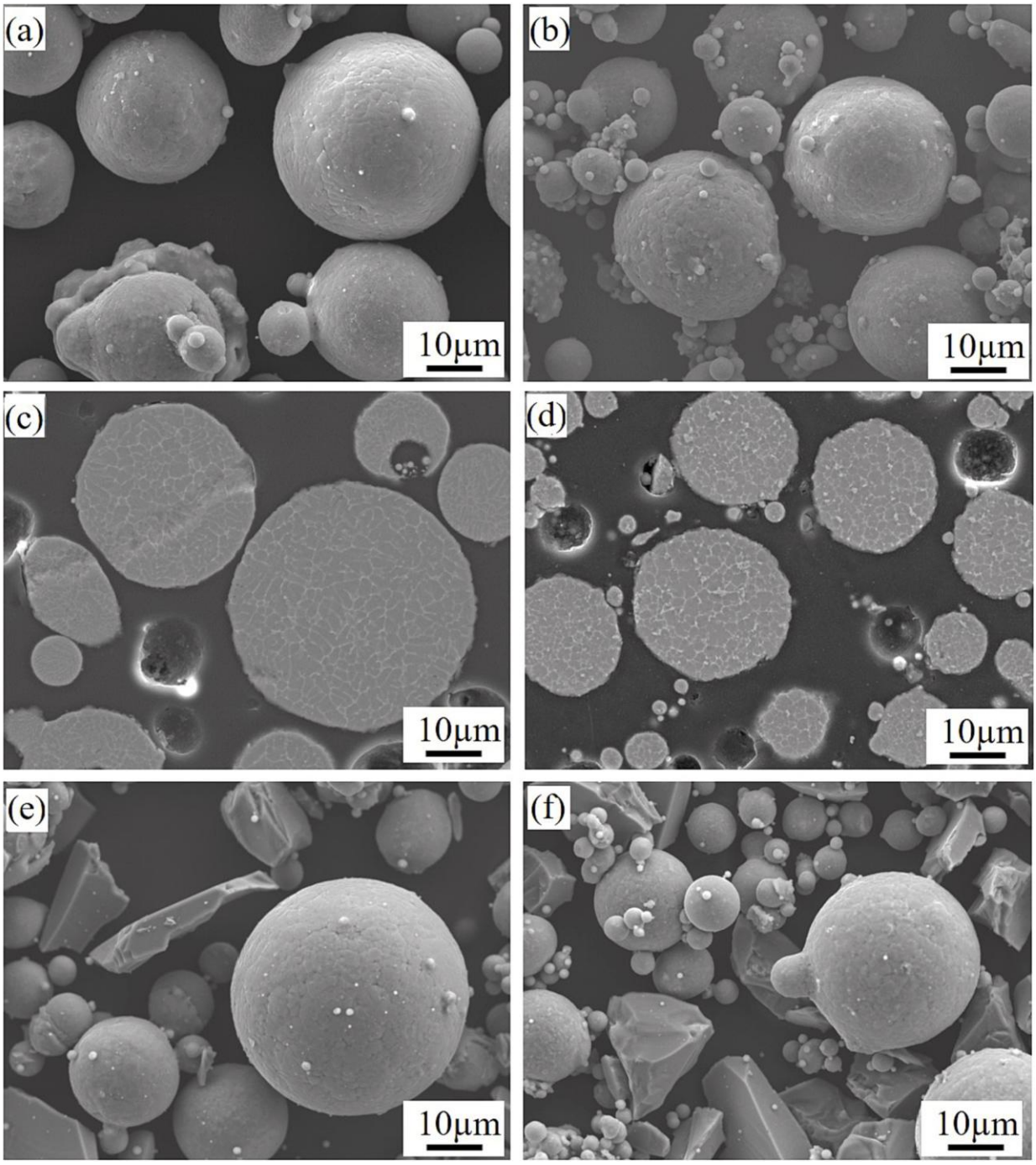


**Fig. 1.** Powder morphologies obtained by SEM: (a) 7075Al, (b) $TiB_2$/7075Al, (e) 7075Al-SiC, (f) TiB2/7075Al-SiC; Cross-sectional micrographs of particles by SEM: (c) 7075Al, (d) TiB2/7075Al.

mm/min. For each deposition condition, four samples were tested for adhesion to obtain an average value.

### *2.5. Tribological test*

Dry sliding wear tests were performed with a CSEM tribometer implement (Switzerland) at ambient temperature. An alumina ball was used as the counter material with a diameter of 6 mm. Different sets of values of the rotating speeds and normal load were used for the friction test: different speeds (2, 5, 10 and 15 cm/s) under the same load (2 N), and different loads (2, 5 and 10 N) under the same linear speed (10 cm/s). The wear track followed a circular path with a diameter of 4 mm and a sliding distance of 300 m. The friction force was measured by a sensor and dynamically recorded by the computer s. The values of the coefficient of friction (COF) were obtained by dividing the measured frictional force with the applied load. After each friction test, the cross-sectional area of the worn traces was measured by an Altisurf 500 profilometer (France). The worn volumes of the samples were calculated as the product between the cross-sectional areas and length of the wear tracks. Afterwards, the surfaces of the worn samples were observed and analyzed by SEM and EDS.

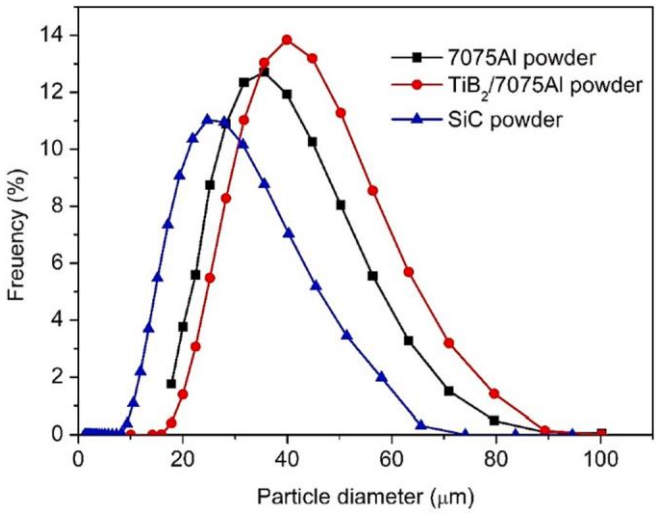


**Fig. 2.** Size distribution of the three powders used.

## 3. Results and discussions

### 3.1. Microstructure

Fig. 3 illustrates the magnified surface morphologies of the 7075Al-SiC and $TiB_2$/7075Al-SiC composite coatings sprayed by CS. Similar deposition features can be observed in the overview morphology of both coatings. The surfaces of both coatings had some globular and irregular protrusions. These could be particles that had not yet been fully deformed (without the impact of subsequent particles resulting in less deformation) and the bonding of these particles might not be very good. Besides, traces can be observed left by some bouncing particles (indicated by red arrows). This was caused by particle rebounds, or shot peening (in the case of hard SiC particles). Some SiC particles may break off during deposition and then leave the coatings or become embedded between the boundaries of the deposited particles. Similar results can be found in the works published by Lee [26] and Kumar [18] studying Al-SiC composite coatings. In addition, it can be seen from the EDS map image in Fig. 3(d) that the nano$TiB_2$ particles were well retained in the TiB2/7075Al-SiC composite coating after deposition.

Fig. 4 shows the cross-section of the coating/substrate interface after polishing. All coatings exhibited considerable denseness and were free of cracks. According to the image contrast, it can be seen that the reinforcing particles were uniformly distributed within the 7075Al-SiC and $TiB_2$/7075Al-SiC coatings and no significant delamination of the particles from the matrix was observed (as shown in Fig. 4(c) and (d), respectively). This is very important for the composite performance as a uniformly distributed hard phase prevents the creation of weak zones. Besides, the interfaces between the coatings and the substrates showed mutual jagged embedment. Fig. 5 illustrates cross-sectional OM magnification images of corroded coatings in three different planes. The micrographs reveal typical jet-type shapes and elongated morphologies. Some severely deformed particles, as well the inter-particle boundaries and grain boundaries were clearly observed. Besides, SiC particulates were well distributed inside the 7075Al-SiC and $TiB_2$/7075Al-SiC

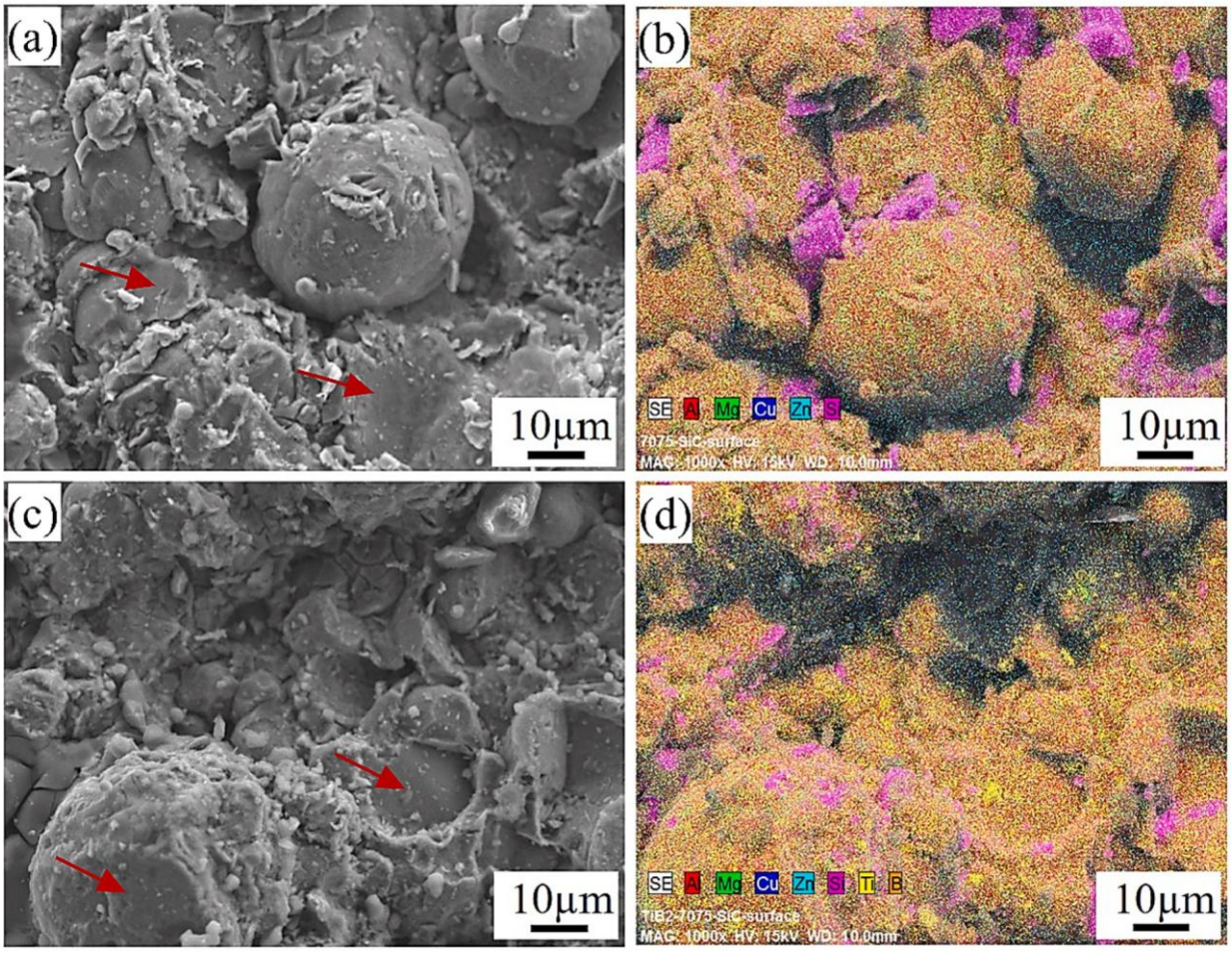


**Fig. 3.** Coating surface morphologies: (a) 7075Al-SiC and (c) its corresponding EDS map, (b) $TiB_2$/7075Al-SiC and (d) its corresponding EDS map.

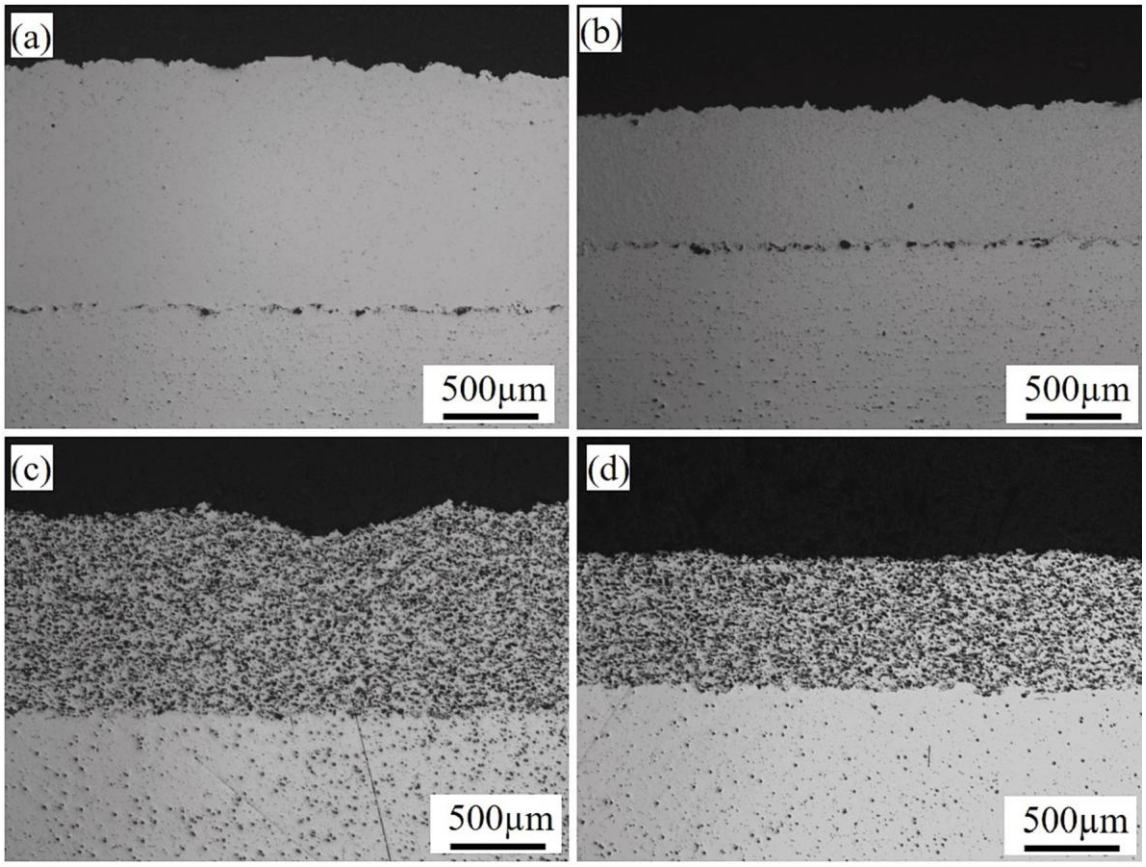


**Fig. 4.** Optical micrographs (OM) of cross sections: (a) pure 7075Al, (b) $TiB_2$/7075Al, (c) 7075Al-SiC and (d) $TiB_2$/7075Al-SiC CS coatings.

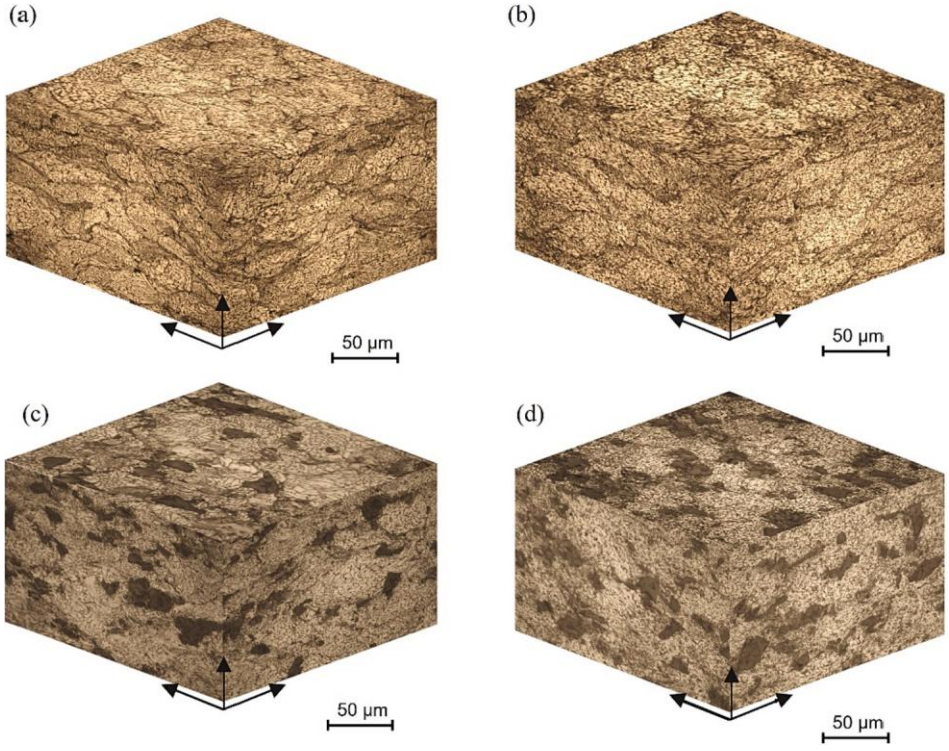


**Fig. 5.** Etched microstructure: (a) pure 7075Al, (b) TiB2/7075Al, (c) 7075Al-SiC and (d) TiB2/7075Al-SiC coatings.

composite coatings. The successful formation of the ceramic particles in the CS coatings was explained by the mechanical "wedging" and subsequent "riveting" effects performed by the metal particles of the sprayed mixture [27,28].

SEM/EDS characterization was also performed to further investigate the microstructure evolution of the different CS coatings, as showed in Fig. 6. It can be seen that the pure 7075 Al and $TiB_2$/7075Al particles were largely deformed during deposition, forming a very dense structure except for the presence of some small pores at the inter-particle regions. SiC particles could be used as in-situ hammering or shot peening particles during the CS deposition, which further deform the metal matrix and produce a process hardening effect on the composite coating. However, SiC is a hard and brittle material; therefore the large, hard-to-deform SiC particles might break off to form pores at the 7075 Al-SiC and $TiB_2$/7075Al-SiC boundary. In addition, as revealed by the SEM (Fig. 5 f and h) and EDS mappings (Fig. 7 e), ultrafine $TiB_2$ particles (and also nanosized ones, but not identifiable at this scale) were uniformly dispersed in the 7075 Al matrix. These irregular $TiB_2$ particles appeared to be dispersed not only inside the deformed particles but also along the interparticle boundaries. Furthermore, we also measured the volume fraction of the ceramic particles in both the $TiB_2$/7075Al and $TiB_2$/7075Al-SiC composite coatings on five SEM images using the Image J software. The volume fraction of $TiB_2$ particles in both composite coatings was about 4.2 vol%, which was the same value as in the composite powder. The SiC content retained in the composite coatings was about 26 vol%, slightly lower than that in the mixed composite powder (30 vol%). Besides, the average SiC particle size within the composite coatings was about 19 μm, which was smaller than that of the initial powder, as a result of their break-off during the CS process.

### 3.2. *Microhardness and nanoindentation*

Fig. 8 shows the microhardness of the different CS coatings produced in this work. The microhardness of composite 7075Al coatings was higher than that of the pure 7075Al. The hybrid reinforced $TiB_2$/7075 Al-SiC composite coatings exhibited a higher microhardness among all coatings. This was related to the content of the reinforcing phase. The in-situ formed TiB2 nanoparticles could be dispersion strengthening materials, while the introduction of more hard SiC particles considerably increased the average hardness of the coating. In addition to the effect of the hardness of the reinforcing phase itself, these particles also had the potential to further plasticize the matrix material and to a certain extent had a shot peening effect on the coatings. In addition, the microhardness measured on the cross-section of the coatings was higher than that on the top surface of the coatings. This might be due to the fact that the cross-section belonged to the interior of the coatings, where there was more extensive plastic deformation and a more concentrated density of dislocations. The location near the top surface had less opportunity to be compacted by subsequent particle impacts and therefore the particles were not deformed to a greater extent than in the interior of the coating at the cross-section. Furthermore, the effect on the hardness of the material during mechanical polishing cannot be exclude. Weakly bonded particles, including the reinforcement SiC, on the top surface could be easily removed, resulting in a local reduction of the volume fraction of the reinforcement. While the inner part of the coatings had a more complex mechanical embedding structure which could lock the SiC particles firmly in place so that they couldn't be easily removed during processing.

Fig. 9 shows the average hardness and modulus values of the different CS coatings measured by the nanoindentation test. The composite coatings exhibited relatively higher hardness and modulus. On the one hand, in coatings possessing TiB2/7075 Al particles, the dispersion strengthening effect of nano $TiB_2$ particles resulted in a higher measured hardness than in the pure 7075 Al coatings. On the other hand, the addition of more hard particles of SiC further increased the average hardness and modulus of the composite coatings. The associated reasons should be similar to those used for analysing the Vickers hardness results. However, these two different indentation tests might lead to varying deviations in the results. For example, the Vickers hardness indenter can produce a larger imprint. Also, measuring at different locations allowed to guarantee the averaging of the particle concentration. The calculated average should be close to the overall hardness level of the coatings. In contrast, the tiny imprint of the nanoindentation could not guarantee the average concentration of particles tested. If the indentation was more on the reinforced particles, the measured hardness and modulus data could be on the high side, resulting in a potentially large deviation in the final average results. Therefore, it is debatable to use such test. Nevertheless, the trending result that the hardness of the coating increases with the addition of reinforcing phase particles should be correct.

In short, 7075Al particles experience significant plastic deformations during spraying. Such strong plastic deformations with high strain/strain rate led to an increase in the density of dislocations, in grain thinning and thus causes work hardening, which has been documented in previous works. Besides, nano $TiB_2$ particles serve as dispersion strengtheners both in the $TiB_2$/7075 Al and $TiB_2$/7075 Al-SiC composite coatings. As for the 7075 Al-SiC and $TiB_2$/7075 Al-SiC coatings, the preservation of the SiC particles integrity and their grit-blasting effect further increase the hardness of the coatings. These effect are in fact the general strengthening mechanisms that prevail when CS is used to prepare particle-reinforced composite coatings [9,29,30]. In addition, the use of indentation testing may require attention to more general

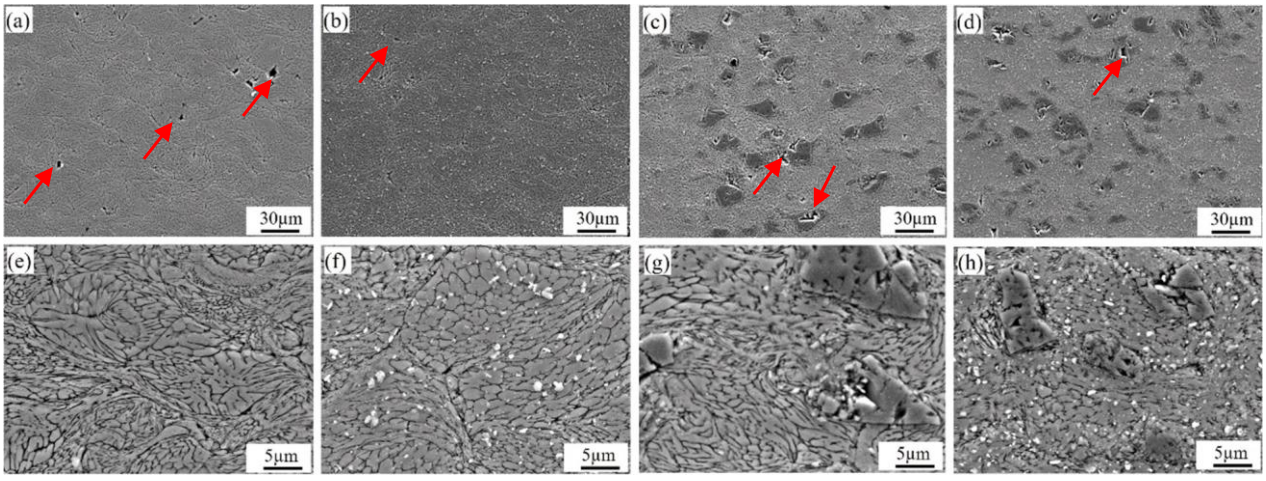


**Fig. 6.** SEM micrographs of the etched cross-sections of (a, e) pure 7075Al, (b, f) $TiB_2$/7075Al, (c, g) 7075Al-SiC and (d, h) $TiB_2$/7075Al-SiC coatings.

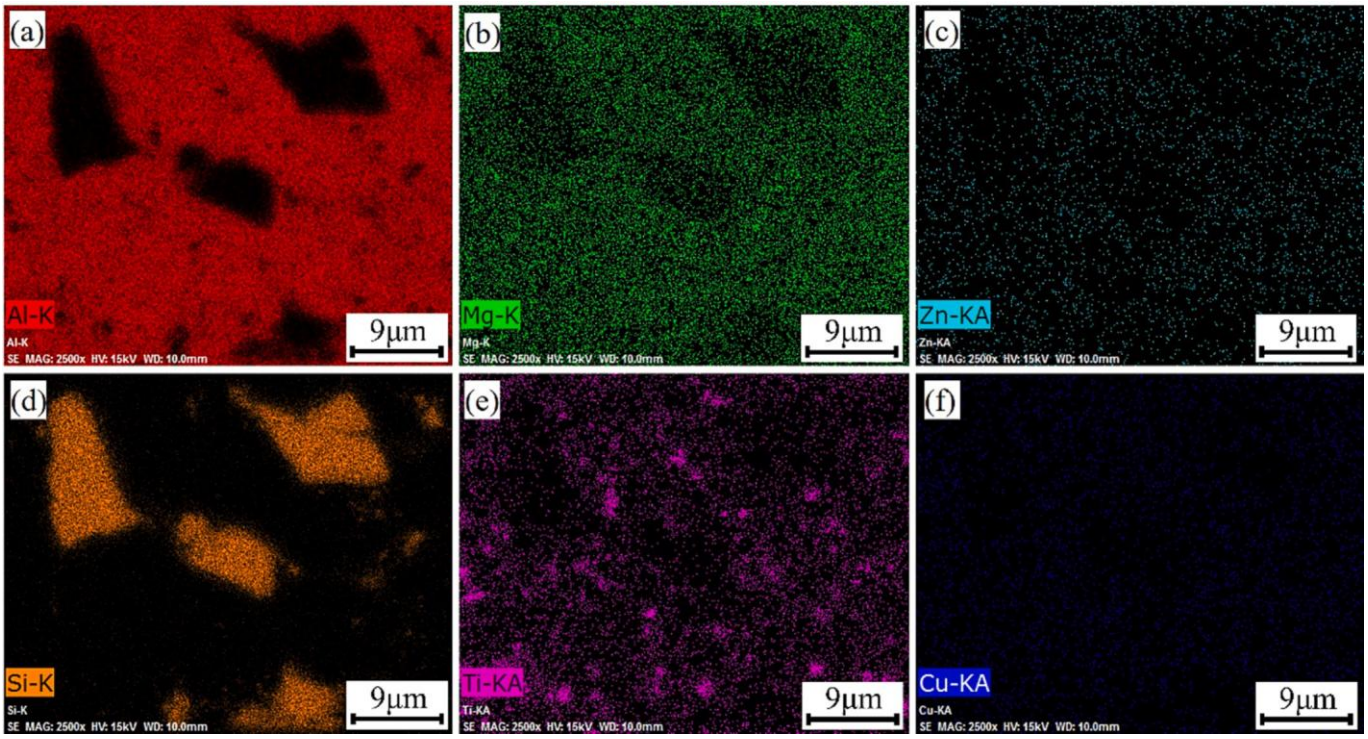


**Fig. 7.** EDS mappings of $TiB_2$/7075Al-SiC coatings.

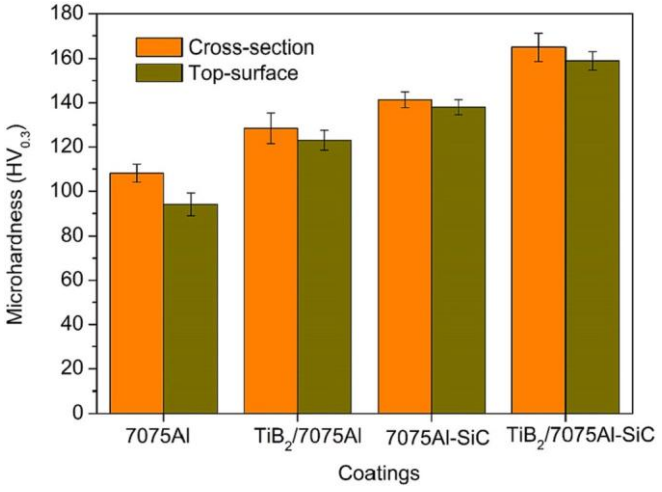


**Fig. 8.** Microhardness data of different coatings obtained with Vickers hardness test method.

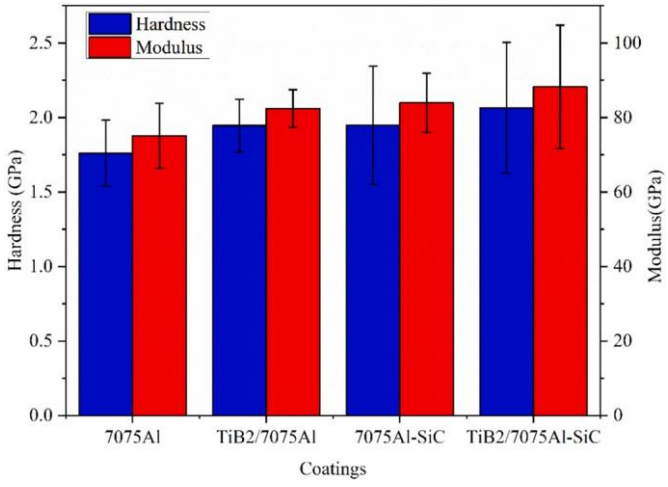


**Fig. 9.** Hardness and modulus data of different coatings by nanoindentation.

rules during operation, which are also some of the challenges that need to be faced in assessing the properties associated with composites [31,32].

### 3.3. Bonding strength

Fig. 10 illustrates the measured adhesion strength data of the different coatings along the coating/substrate interface, as obtained through the tensile pull-off adhesion testing. Compared to pure 7075Al, the adhesion strength of the composite coatings had been improved. Moreover, the introduction of SiC particles seemed to help strengthen the adhesion of the coating even more. As mentioned above, the initial coating/substrate bonding process developed in the CS process is due to embedding. The adhesion strength essentially depends on severe plastic deformations of the spray particles, and is caused by material interlocking and mechanical intermingling between the corresponding atoms of the substrate and the coating powder [8,9]. Previous studies have led to the conclusion that together the particle impact velocity, the particle or substrate temperature, the substrate roughness and the particle morphology play important roles in improving the adhesion strength resulting from plastic deformation [33–36].

The $TiB_2$ nanoparticles were rather small and had a low volume fraction in the coating, and most of them were uniformly distributed inside the particles. Its effect on the mechanical interlocking and metallurgical bonding between the coating and the substrate was less then SiC. The addition of SiC particles could further increase the adhesion strength of the 7075Al-SiC and $TiB_2$/7075Al-SiC composite coatings. On the one hand, the impact of some SiC particles could produce a grit-blasting effect that might in some way increase the roughness of the

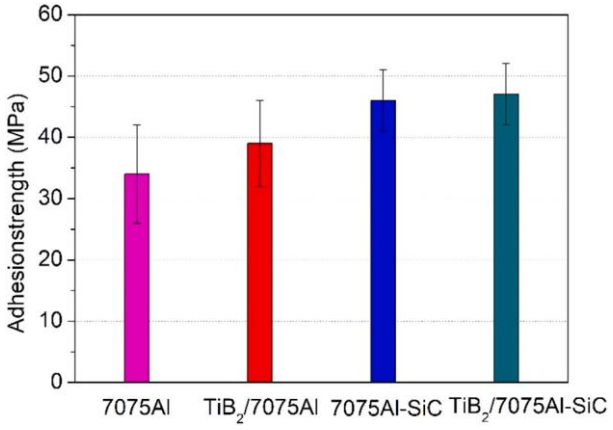


**Fig. 10.** The adhesion strengths of different coatings.

substrate surface. On the other hand, in the coating deposition process, the shot-peening effect of some SiC particles also increased the plastic deformation of the metal particles. Both effects were conducive to the mechanical interlocking process, leading to better adhesion between the composite coating and the substrate. In general, the addition of ceramic particles can increase the adhesion strength of the coating by cold spray, as the micron-sized hard ceramic particles can enhance the deformation of the soft metal particles and thus increase the quality of the bonding [28,37]. However, when the volume fraction of the ceramic particles reaches a high level (>50 vol%), the adhesion strength remains stable or even starts to decrease. The fact that the particles allow for strong plastic deformation is one of the prerequisites for the successful deposition of CS. The increase in hard particles reduces the relative content of the aluminium matrix, resulting in a lower proportion of bonding due to deformation. In this study, the SiC volume fraction was <30% ensuring that the deformable matrix dominated in terms of volume ratio, thus avoiding such a problem.

### 3.4. Tribological performance

Fig. 11 a and b show the values of the coefficient of friction (COF) versus the wear distance obtained for the different CS coatings under different testing condition. Unfortunately, for the 7075Al and $TiB_2$/7075Al samples, the signal fluctuations which appeared during the wear test performed with the higher load/speed parameters were too large to allow a proper evaluation. Only the test with the load of 2 N and the linear speed of 10 cm/s were exploitable, which might be result from the unstable wear mechanisms. It can be assumed that when the load or the linear speed was increased along the contacting surfaces, the two surfaces were prone to stick with each other (locked braking) due to friction heat that was induced by rubbing, thus leading to a high friction behavior. Consequently, the tribological performances of both coatings were negatively impacted. All the COF curves showed an unstable initial state (run-in) in the beginning and then became steady after about 80 m and 50 m sliding distance. As seen in Fig. 11 c, the COF value of the 7075Al-SiC and $TiB_2$/7075Al-SiC samples gradually decrease as the load increases, implying that the composite coating can show better lubricity when subjected to higher loads. Besides, the COF values of both samples were very close under lower loads. When the load was raised, the COF value of $TiB_2$/7075Al-SiC sample proved to slightly exceed - that of the 7075Al-SiC. Fig. 11 d shows the COF values of 7075Al-SiC and $TiB_2$/7075Al-SiC samples under a load of 2 N and for different rotation speeds. It is found that their COF values first increased and then decreased as the rotation speed increases, and gradually approached each other.

Fig. 12 shows the wear rate of the 7075Al-SiC and $TiB_2$/7075Al-SiC coatings under different testing conditions. It can be seen that as the load or line speed increased, the coating wear rate decreased. Besides, $TiB_2$/7075Al-SiC had a lower wear rate than 7075Al-SiC under the same conditions. This means that $TiB_2$/7075Al-SiC coating underwent less wear and could be expected to have a longer service life.

Overall, the microhardness and adhesion strength of the composite coatings were increased by incorporating ceramic particles of SiC and nano-$TiB_2$ into an Al matrix, resulting in improved tribological performances. However, it seems that adding SiC particles had a more

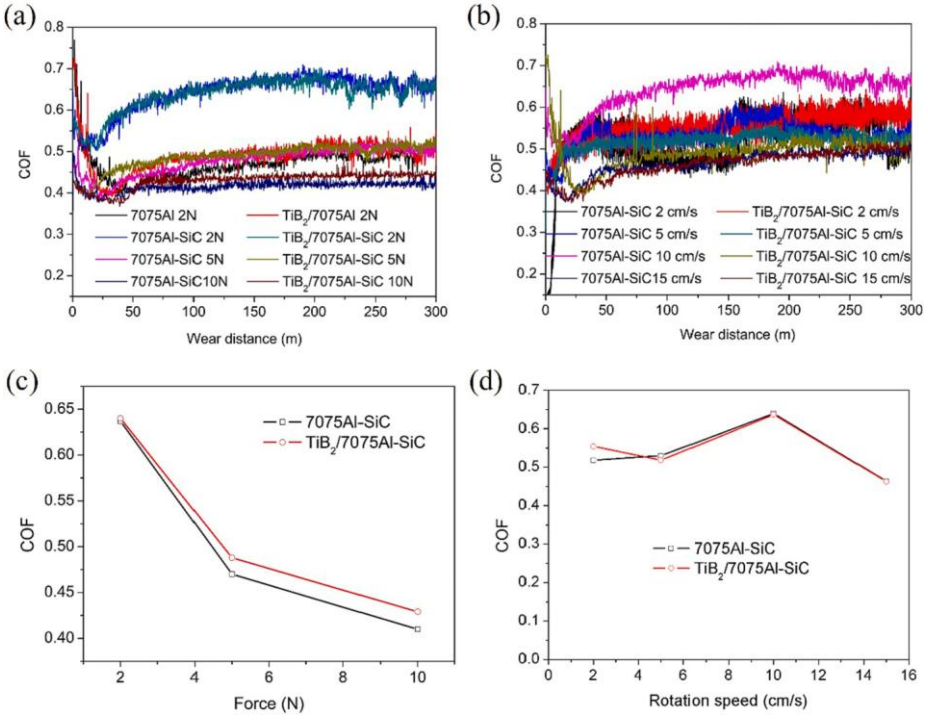


**Fig. 11.** (a) COF curves and (c) COF values of the different coatings under the loads of 2, 5 and 10 N and the same linear speed (10 cm/s); (b) COF curves and (d) COF values of the different coatings under the speeds of 2, 5, 10 and 15 cm/s and the same load (2 N).

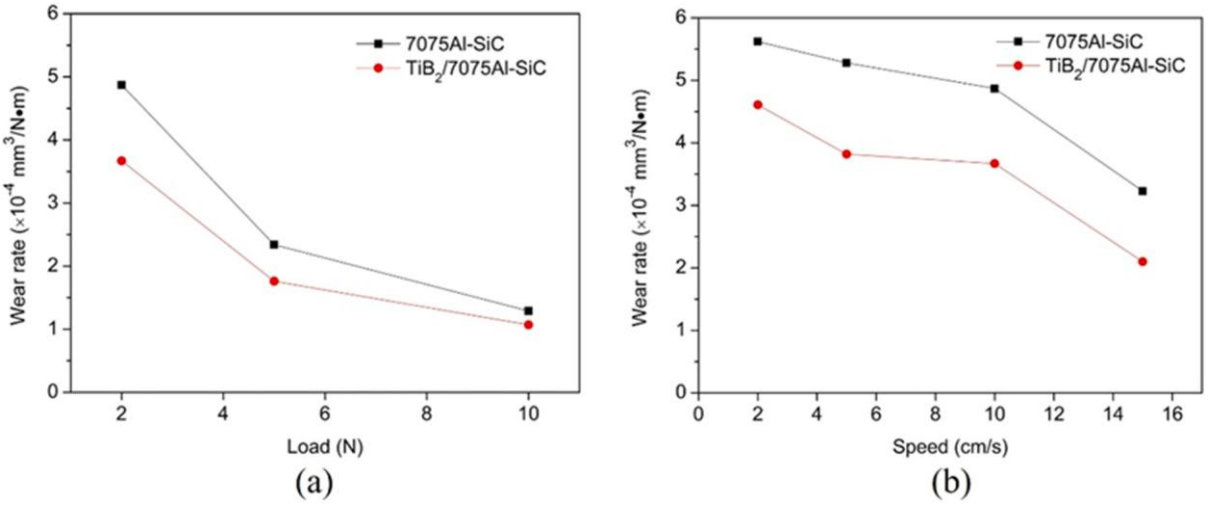


**Fig. 12.** Wear rate of 7075Al-SiC and $TiB_2$/7075Al-SiC coatings under (a) different loads (2, 5 and 10 N) and the same linear speed (10 cm/s); (b) different speeds (2, 5, 10 and 15 cm/s) and the same load (2 N).

significant influence on the COF of the material than adding $TiB_2$ particles. This might be related to the type, content, structure and size of these very distinct ceramic particles. Thus, the lubricity of the material was only slightly influenced by the modest amount of $TiB_2$ particles present. However, compared to the 7075Al-SiC composite sample, the incorporation of nano-$TiB_2$ particles dispersed inside the $TiB_2$/7075 Al-SiC coating facilitated further improvements in the wear life of the material.

### *3.5. Wear track and debris analysis*

To understand the experimental results and the wear mechanisms, the worn surfaces of the three CS coatings were examined by SEM. The images obtained under a load of 2 N and a linear speed of 10 cm/s are presented in Fig. 13. It can be seen that, when the content of ceramic particles increases, the width of the wear track on the surface of the coating became narrower. This could be due to the increase in hardness. The worn surface of the 7075Al coating (Fig. 13(a) and (e)) revealed a typical feature of adhesive wear exhibiting a larger plastic flow. Besides, the wear track profiles show traces of extrusion of the worn material outside the furrow. The $TiB_2$/7075Al coating (Fig. 13(b) and (f)) exhibited a similar wear pattern to that of the 7075Al coating. Although the $TiB_2$/7075Al coating contained lubricious $TiB_2$ nanoparticles which had a certain strengthening effect on the coating, its content was relatively low. Thus, the worn surface of the coating was still dominated by adhesive wear. The worn surfaces of the 7075Al-SiC (Fig. 13(c)) and $TiB_2$/7075Al-SiC coatings (Fig. 13(d)) displayed clear grooves running parallel to the sliding direction, indicating a wear mechanism dominated by abrasion. Under higher magnification observation, it can be seen the two coatings underwent different intensities of wear scars. Severe traces of abrasive wear and some loose wear debris could be found in the 7075Al-SiC sample. The loss of material suffered by the $TiB_2$/7075Al-SiC coating seemed to be lower. This can be tentatively attributed to ploughing caused by weak bonding strength particles which was torn out of the matrix, particularly the SiC particles. The interfacial bonding between matrix and reinforcement materials might be weak. The reinforcement was removed due to failure at the matrix/reinforcement interface. Over time, more and more particles might be released into the friction interface, leading to unfavorable three-body wear and also to significant delamination of the ceramic particles from the matrix. For TiB2/7075Al-SiC coating, the in-situ nano-$TiB_2$ in the matrix was not readily ploughed off and acted as a diffuse reinforcer to reduce the effect of abrasive wear by SiC particles. Fig. 14 shows the composition of the worn surfaces of 7075Al-SiC and TiB2/7075Al-SiC. It can be seen that the ploughed-out SiC particles were pushed into a more concentrated position on the worn surface of 7075Al-SiC, while they still

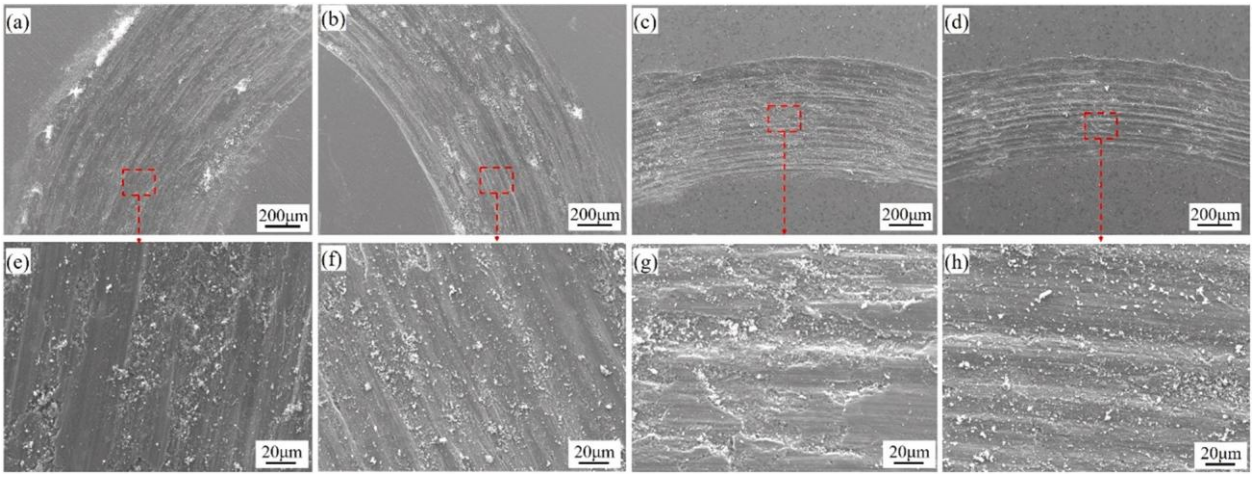


**Fig. 13.** Wear track morphologies of (a) (e) 7075Al; (b) (f) $TiB_2$/7075Al; (c) (g) 7075Al-SiC; (d) (h) $TiB_2$/7075Al-SiC under a load of 2 N and a linear speed of 10 cm/s.

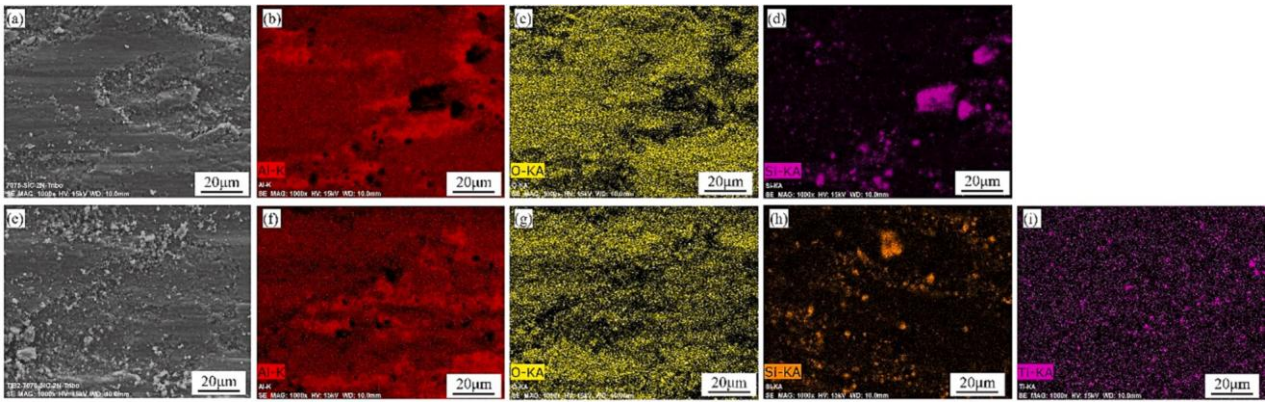


**Fig. 14.** EDS mappings of the wear track of (a, b, c, d) 7075Al-SiC and (e, f, g, h, i) $TiB_2$/7075Al-SiC under a load of 2 N and a linear speed of 10 cm/s.

were evenly dispersed in the worn surface of TiB2/7075Al-SiC. It seems that SiC was more likely to be ploughed out in the 7075Al-SiC coating, while nano $TiB_2$ in the TiB2/7075Al-SiC coating could act as a barrier to the wear by SiC that might be ploughed out.

Fig. 15 shows SEM views of the worn surface of 7075Al-SiC and $TiB_2$/7075Al-SiC coatings under the load of 10 N and the linear speed of 10 cm/s. In comparison to the worn surface developed under lower load in Fig. 12(c) and (d), the worn surfaces under higher load are smoother and the removals of material are less pronounced. The $TiB_2$/7075Al-SiC coating undergoes less material loss than the 7075 Al-SiC coating. This might be because with the increase in friction load, the increase in temperature of friction surface leads to a decrease in the strength of the material. The softening of low melting point metal, on one hand, and the creation of oxide films by friction at increased temperatures, on another hand, cause a reduction of the friction coefficient, thereby reducing the loss of material. In addition, the weaker bound ceramic particles, particularly for SiC, were rapidly released into the friction interface under high loads, while the larger particles were crushed and refined. This can be seen in the results of the compositions on the worn surface in Fig. 16. $TiB_2$ particles might also be partially ploughed out under high loads. These fine ceramic particles (mainly SiC) behaved as abrasive agents during friction and thus reduced the friction coefficient.

## 4. Conclusions

In this study, hybrid particles of nano-in-situ $TiB_2$ and micro-SiC were incorporated into 7075Al matrix and the corresponding advanced AMCs were successfully produced by CS. Microstructure and mechanical properties, including hardness, adhesion strength, wear resistance, were investigated and compared with other coatings. The main conclusions drawn from this work are as follows:

(1) The in-situ formed nano-$TiB_2$ particles were well preserved in the composite coating. They were not only dispersed inside the deformed particles, but also along the inter-particle boundaries. The content of the mechanically mixed SiC particles was slightly

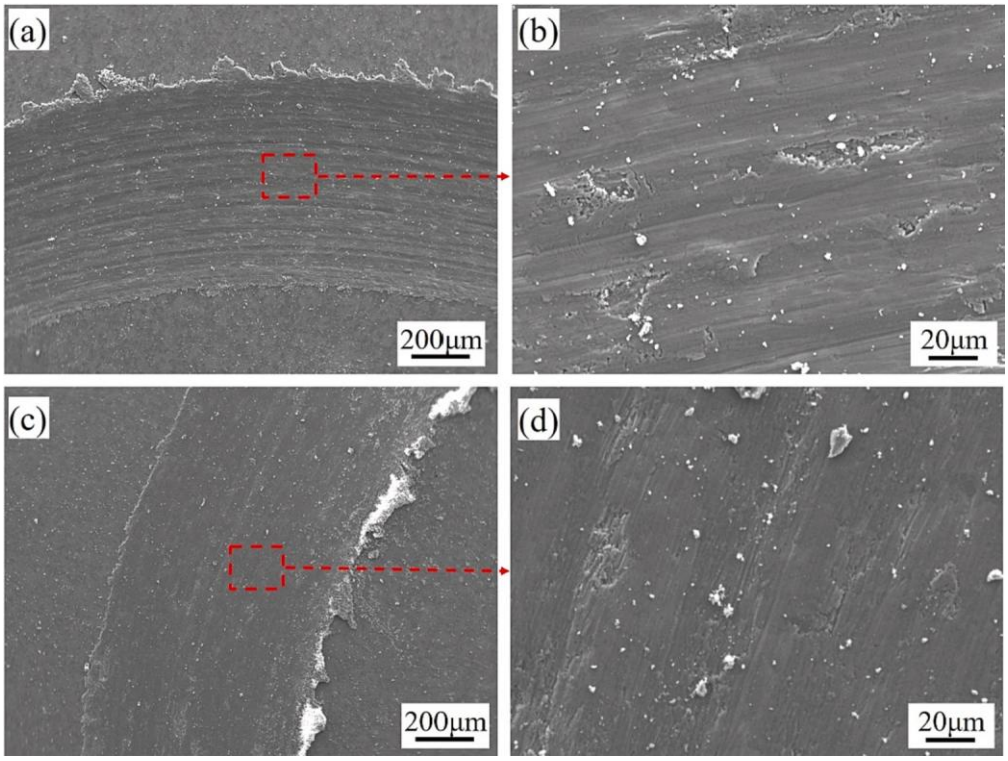


**Fig. 15.** Wear track morphologies of (a) (b) 7075Al-SiC; (c) (d) $TiB_2$/7075Al-SiC under a load of 10 N and a linear speed of 10 cm/s.

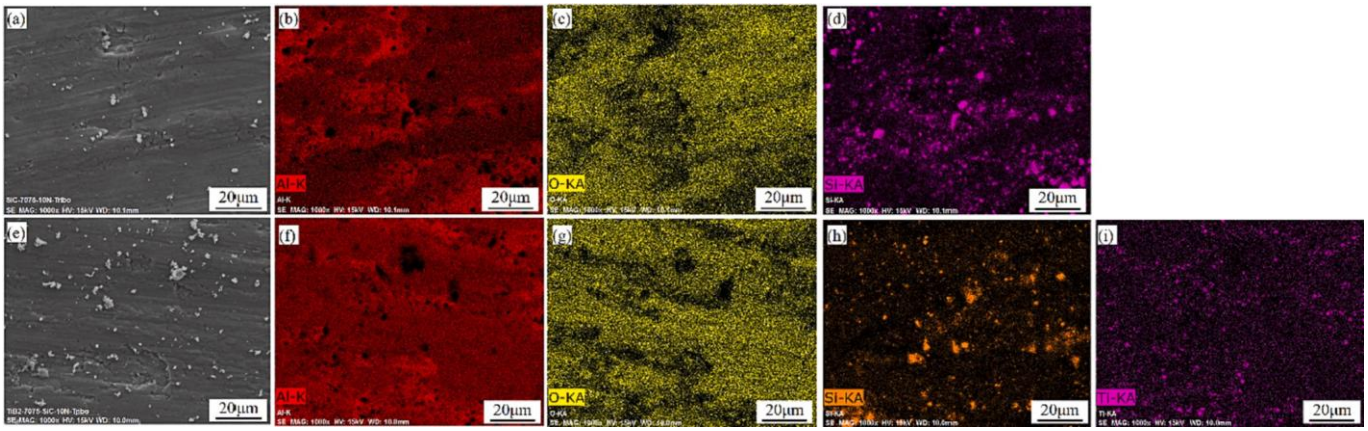


**Fig. 16.** EDS mappings of the wear tracks of (a, b, c, d) 7075Al-SiC and (e, f, g, h, i) $TiB_2$/7075Al-SiC under a load of 10 N and a linear speed of 10 cm/s. (Note: very fine and uniformly distributed SiC particles).

reduced during the deposition of the coating. SiC can perform the effect of shot blasting to improve the coating density.

(2) The mechanical properties of 7075Al-based composite coatings, including hardness, modulus and adhesion strength, were higher than those of pure 7075Al coatings. The in-situ formed nano-$TiB_2$ particles produced a dispersion strengthening effect. The SiC particles played a key role in increasing the hardness of the composite coatings and enhancing its bonding to the substrate. When both types of ceramic particles were added together to the 7075Al coating, the increased content of the reinforcing phase led to a greater enhancement of the mechanical properties of TiB2/7075Al-SiC composite coatings.

(3) Pure 7075 Al and $TiB_2$/7075 Al coatings mainly displayed an adhesive wear behavior during the friction process, while the 7075 Al-SiC and $TiB_2$/7075 Al-SiC composite coatings exhibited abrasive wear. The type of ceramic, its content and distribution, as well as the bonding properties with the matrix determined the wear behavior of the coatings. $TiB_2$/7075Al-SiC composite coatings exhibited better wear resistance. The in-situ formed nano-$TiB_2$ particles increased the hardness of the matrix, and they were not easy to be ploughed off during the friction process, instead they could hinder the abrasive behavior of the SiC particles. In addition, the friction parameters had a significant impact on the wear performance of the composite coatings. Under high load or high-speed friction, an oxide film was more likely to form on the friction surface. Besides, weakly bound particles were rapidly separated into the friction interface and larger hard particles were crushed and refined. These contributed to reducing the friction coefficient of the composite coatings.

## CRediT authorship contribution statement

**Xinliang Xie**, **Hanlin Liao:** Conceptualization, Methodology, Software. **Shaowu Liu**, **Hongjian Wu:** Data curation, Writing - Original draft preparation. **Xinliang Xie:** Visualization, Investigation. Supervision. **Michel Moliere**, **Gang Ji:** Writing - Reviewing and Editing

## Declaration of competing interest

The authors declare that they have no known competing financial interests or personal relationships that could have appeared to influence the work reported in this paper.

## Data availability

The authors are unable or have chosen not to specify which data has been used.

## Acknowledgements

The authors would like to acknowledge the National Natural Science Foundation of China (No. 52204390).

## References

[1] K.M. Shorowordi, T. Laoui, A. Asm, J.-P. Haseeb, L.Froyen Celis, Microstructure and interface characteristics of B4C, SiC and Al2O3 reinforced Al matrix composites: a comparative study, J. Mater. Process. Technol. 142 (2003) 738–743.
[2] B.V. Ramnath, C. Elanchezhian, R.M. Annamalai, S. Aravind, T.S.A. Atreya, V. Vignesh, C. Subramanian, Aluminium metal matrix composites-a review, Rev. Adv. Mater. Sci. 38 (2014) 55–60.
[3] G. Manohar, A. Dey, K.M. Pandey, S.R. Maity, Fabrication of metal matrix composites by powder metallurgy: a review, in: AIP Conference Proceedings, AIP Publishing LLC, 2018, p. 020041.
[4] V. Auradi, G.L. Rajesh, S.A. Kori, Processing of B4C particulate reinforced 6061Aluminum matrix composites by melt stirring involving two-step addition, ProcediaMater. Sci. 6 (2014) 1068–1076.
[5] M. Dhanashekar, V.S. Kumar, Squeeze casting of aluminium metal matrix composites-an overview, Procedia Eng. 97 (2014) 412–420.
[6] X. Xie, S. Yin, R. Raoelison, C. Chen, C. Verdy, W. Li, G. Ji, Z. Ren, H. Liao, Al matrix composites fabricated by solid-state cold spray deposition: a critical review, J. Mater. Sci. Technol. 86 (2021) 20–55.
[7] T.W. Clyne, P.J. Withers, An Introduction to Metal Matrix Composites, Cambridge University Press, 1995.
[8] A. Papyrin, V. Kosarev, S. Klinkov, A. Alkhimov, V.M. Fomin, Cold Spray Technology, Elsevier, 2006.
[9] V.K. Champagne, The Cold Spray Materials Deposition Process, Elsevier, 2007.
[10] R.N. Raoelison, C. Verdy, H. Liao, Cold gas dynamic spray additive manufacturing today: deposit possibilities, technological solutions and viable applications, Mater. Des. 133 (2017) 266–287.
[11] H. Wu, S. Liu, X. Xie, Y. Zhang, H. Liao, S. Deng, A framework for a knowledge based cold spray repairing system, J. Intell. Manuf. 1–9 (2021).
[12] H. Wu, X. Xie, M. Liu, C. Verdy, Y. Zhang, H. Liao, S. Deng, Stable layer-building strategy to enhance cold-spray-based additive manufacturing, Addit. Manuf. 35 (2020), 101356.
[13] Z. Zhang, F. Liu, E.-H. Han, L. Xu, Mechanical and corrosion properties in 3.5% NaCl solution of cold sprayed Al-based coatings, Surf. Coat. Technol. 385 (2020), 125372.
[14] M. Yandouzi, S. Gaydos, D. Guo, R. Ghelichi, B. Jodoin, Aircraft skin restoration and evaluation, J. Therm. Spray Technol. 23 (2014) 1281–1290, https://doi.org/10.1007/s11666-014-0130-1.
[15] N.H. Tariq, L. Gyansah, J.Q. Wang, X. Qiu, B. Feng, M.T. Siddique, T.Y. Xiong, Cold spray additive manufacturing: a viable strategy to fabricate thick B4C/Al composite coatings for neutron shielding applications, Surf. Coat. Technol. 339 (2018) 224–236.
[16] Y. Tao, T. Xiong, C. Sun, H. Jin, H. Du, T. Li, Effect of α-Al2O3 on the properties of cold sprayed Al/α-Al2O3 composite coatings on AZ91D magnesium alloy, Appl. Surf. Sci. 256 (2009) 261–266.
[17] H.Y. Lee, Y.H. Yu, Y.C. Lee, Y.P. Hong, K.H. Ko, Cold spray of SiC and Al 2 O 3 with soft metal incorporation: a technical contribution, J. Therm. Spray Technol. 13 (2004) 184–189.
[18] S. Kumar, S.K. Reddy, S.V. Joshi, Microstructure and performance of cold sprayed Al-SiC composite coatings with high fraction of particulates, Surf. Coat. Technol. 318 (2017) 62–71.

[19] M. Yu, X.K. Suo, W.Y. Li, Y.Y. Wang, H.L. Liao, Microstructure, mechanical property and wear performance of cold sprayed Al5056/SiCp composite coatings: effect of reinforcement content, Appl. Surf. Sci. 289 (2014) 188–196.
[20] S. Pan, T. Saso, N. Yu, M. Sokoluk, G. Yao, N. Umehara, X. Li, New study on tribological performance of AA7075-TiB2 nanocomposites, Tribol. Int. 152 (2020), 106565.
[21] X. Xie, B. Hosni, C. Chen, H. Wu, Y. Li, Z. Chen, C. Verdy, O.E. Kedim, Q. Zhong, A. Addad, Corrosion behavior of cold sprayed 7075Al composite coating reinforced with TiB2 nanoparticles, Surf. Coat. Technol. 404 (2020), 126460.
[22] X. Xie, Y. Ma, C. Chen, G. Ji, C. Verdy, H. Wu, Z. Chen, S. Yuan, B. Normand, S. Yin, Cold spray additive manufacturing of metal matrix composites (MMCs) using a novel nano-TiB2-reinforced 7075Al powder, J. Alloys Compd. 819 (2020), 152962.
[23] A.B. Gurcan, T.N. Baker, Wear behaviour of AA6061 aluminium alloy and its composites, Wear 188 (1995) 185–191.
[24] H.C. Park, Wear behavior of hybrid metal matrix composite materials, Scr. Metall. Mater. 27 (1992) 465–470.
[25] H. Ahlatci, T. Kocer, E. Candan, H. Çimenoğlu, Wear behaviour of Al/(Al2O3p + SiCp) hybrid composites, Tribol. Int. 39 (2006) 213–220.
[26] H. Lee, K. Ko, Effect of SiC particle size on cold sprayed Al–SiC composite coatings, Surf. Eng. 25 (2009) 606–611.
[27] R. Chakrabarty, J. Song, Numerical simulations of ceramic deposition and retention in metal-ceramic composite cold spray, Surf. Coat. Technol. 385 (2020), 125324, https://doi.org/10.1016/j.surfcoat.2019.125324.
[28] Q. Wang, K. Spencer, N. Birbilis, M.-X. Zhang, The influence of ceramic particles on bond strength of cold spray composite coatings on AZ91 alloy substrate, Surf. Coat. Technol. 205 (2010) 50–56.
[29] H. Wu, C. Huang, X. Xie, S. Liu, T. Wu, T. Niendorf, Y. Xie, C. Deng, M. Liu, H. Liao, S. Deng, Influence of spray trajectories on characteristics of cold-sprayed copper deposits, Surf. Coat. Technol. 405 (2021), 126703, https://doi.org/10.1016/j.surfcoat.2020.126703.
[30] R.C. Dykhuizen, M.F. Smith, D.L. Gilmore, R.A. Neiser, X. Jiang, S. Sampath, Impact of high velocity cold spray particles, J. Therm. Spray Technol. 8 (1999) 559–564, https://doi.org/10.1361/105996399770350250.
[31] P. Jenczyk, H. Grzywacz, M. Milczarek, D.M. Jarząbek, Mechanical and tribological properties of co-electrodeposited particulate-reinforced metal matrix composites: a critical review with interfacial aspects, Materials. 14 (2021) 3181.
[32] P. Jenczyk, M. Gawrońsk, M. Milczarek, W. Dera, J. Chrzanowska-Giżyńska, P. Denis, D.M. Jarząbek, Application of SiC particles coated with a protective ni layer for production of Ni/SiC co-electrodeposited composite coatings with enhanced tribological properties, Ceram. Int. 45 (17) (2019) 23540–23547.
[33] T. Noguchi, A. Magario, S. Fukazawa, S. Shimizu, J. Beppu, M. Seki, Carbon Nanotube/Aluminium composites with uniform dispersion, Mater. Trans. 45 (2004) 602–604, https://doi.org/10.2320/matertrans.45.602.
[34] A.M.K. Esawi, K. Morsi, A. Sayed, A.A. Gawad, P. Borah, Fabrication and properties of dispersed carbon nanotube–aluminum composites, Mater. Sci. Eng. A 508 (2009) 167–173, https://doi.org/10.1016/j.msea.2009.01.002.
[35] A. Esawi, K. Morsi, Dispersion of carbon nanotubes (CNTs) in aluminum powder, Compos. A: Appl. Sci. Manuf. 38 (2007) 646–650, https://doi.org/10.1016/j.compositesa.2006.04.006.
[36] H. Kwon, M. Estili, K. Takagi, T. Miyazaki, A. Kawasaki, Combination of hot extrusion and spark plasma sintering for producing carbon nanotube reinforced aluminum matrix composites, Carbon 47 (2009) 570–577, https://doi.org/10.1016/j.carbon.2008.10.041.
[37] A. Sova, A. Papyrin, I. Smurov, Influence of ceramic powder size on process of cermet coating formation by cold spray, J. Therm. Spray Technol. 18 (2009) 633–641, https://doi.org/10.1007/s11666-009-9359-5.